Appl. Phys. B 58, 183–195 (1994)

Applied Physics B Lasers and Optics

Femtosecond Hybrid Mode-Locked Semiconductor Laser and Amplifier Dynamics

P. J. Delfyett[1], **A. Dienes**[2], **J. P. Heritage**[2], **M. Y. Hong**[2], **Y. H. Chang**[2]

[1] Center for Research and Education in Optics & Lasers, Electrical & Computer Engineering, University of Central Florida, Orlando, FL, 32826, USA (Tel.: +407/658-6812, e-mail: delfyett@admin.creol. ucf.edu)
[2] Department of Electrical and Computer Engineering, University of California, Davis, CA 95616, USA (Fax: +1-916/752-8428)

Received 15 July 1993/Accepted 20 November 1993

Abstract. We describe the generation of femtosecond high power optical pulses using hybrid passive-active mode-locking techniques. Angle stripe geometry GaAs/AlGaAs semiconductor laser amplifiers are employed in an external cavity including prisms and a stagger-tuned quantum-well saturable absorber. An identical amplifier also serves as an optical power amplifier in a stretched pulse amplification and recompression sequence. After amplification and pulse compression this laser system produces 200 fs, 160 W peak power pulses. We discuss and extend our theory, and supporting phenomenological models, of picosecond and subpicosecond optical pulse amplification in semiconductor laser amplifiers which has been successful in calculating measured spectra and time-resolved dynamics in our amplifiers. We have refined the theory to include a phenomenological model of spectral hole-burning for finite intraband thermalization time. Our calculations are consistent with an intraband time of approximately 60 fs. This theory of large signal subpicosecond pulse amplification will be an essential tool for understanding the mode-locking dynamics of semiconductor lasers and for analysis of high speed multiple wavelength optical signal processing and transmission devices and systems based on semiconductor laser amplifiers.

PACS: 42.55.Px, 42.65.–k

Recent experimental progress in high power modelocked semiconductor lasers [1, 2] has underscored the need for an improved theory of amplification in these devices that correctly accounts for THz bandwidths and high intensities. The experimental art has been advancing rapidly [3–7]. Today, the external cavity, semiconductor laser plus amplifier system described in Sect. 1 produces satellite free, nearly transform limited, 200 fs pulses with over 160 W of peak power. This is an achievement that was only dreamed about three years ago. During the same few years the MIT group [8–13], and others [14, 15] executed a series of elegant experimental measurements of picosecond and subpicosecond gain and phase dynamics. It was found that a subpicosecond pulse saturates the gain of the Semiconductor Laser Amplifier (SLA) more readily than does a picosecond pulse. This property of the SLA has important consequences for wide-bandwidth and high-power SLA applications. The mode-locking processes in the SLA-based short-pulse laser mentioned above is an important example because of the high peak intensity inside the laser resonator and the multi-THz bandwidth required to support an ultrashort pulse. Just as important is the case of mixing of two or more widely separated optical tones such as one will meet in future Wavelength Division Multiplexed (WDM) communications network applications. A thoroughly tested, complete theory of subpicosecond amplification is needed, not just for the knowledge gained about the amplification process, but also because such a theory will be a useful tool in the analysis of broadband optical systems, such as mode-locked lasers and multiple wavelength communications and networking systems that use these amplifiers. This paper will: (1) outline the status of the art of mode-locking using SLA-based ultrashort-pulse systems, and (2) describe progress in the development of the theory of short-pulse amplification in the saturation regime. The laser that we will describe in Sect. 1 includes an intracavity four-prism sequence and a stagger-tuned multiple-quantum-well saturable absorber. Both are required for generation of the wide optical bandwidth. Despite the familiar resonator construction, this laser is quite extraordinary in its performance. The oscillator does not produce a subpicosecond pulse directly. Instead it produces a long ($\approx$10 ps) pulse with an almost perfect linearly chirped spectrum that is $\approx$50 times the transform limit. It is not yet clear how the SLA, the prisms, and the broadband saturable absorber interact to produce a stable, well-organized pulse spectrum. Casually we can say that this laser seems to know what we want: i.e. to produce an ultrashort transform-limited pulse. It cannot do this directly because of the strong subpicosecond gain suppression, so the laser does the next best thing: it generates a long, linearly chirped pulse which can be externally compressed to 200 fs. This singular mode-locking process is not yet understood. What is clear, however, is that a theory of the mode-locking of this laser will need to explicitly consider the large-signal, short-pulse behavior of the SLA.

While we do not present a theory of semiconductor laser mode-locking here we do present, in Sect 2, our theory of the SLA that is a prerequisite to an analytical description of this remarkable laser system. This paper includes recent important enhancements and extensions as well as a revisit to our previous work. Briefly, our theory explicitly accounts for the large-signal behavior of the SLA. It takes into account the dynamic saturation behavior of the gain and refractive index through simple but realistic physical models of carrier-depletion induced and carrier-heating-induced gain and index changes. Also included are the index changes from the nonlinear refractive index and losses including two-photon absorption. The spectral variation of the gain and index are accounted for by a Taylor expansion with the temporal variation of each term included in the form of a simple linearized time dependence. Section 3 documents the success of this theory by comparing to experiments in which ≈400 fs and ≈2 ps optical pulses, derived from the mode-locked laser system described in Sect. 1, are used to interrogate another SLA identical to that used in the source. This comparison of theory and experiment is, to date, the most complete and successful yet published. It documents the rapid progress in experimental and theoretical understanding of the SLA that has been unfolding and improving over the last few years.

1 High Power Mode Locking with Semiconductor Laser Amplifiers

In this section, we discuss the main concepts associated with the production of ultrashort, high power optical pulses from semiconductor laser diodes. The goal is to produce high peak power femtosecond duration optical pulses. In this approach, an external cavity oscillator and a single-stage amplifier design has been employed for several reasons: (1) independent control of the gain and saturable absorption can be achieved, and (2) a lower cavity repetition rate allows for complete gain recovery in both the oscillator and amplifier gain stages. The former reason allows one to assure that the absorber is easier to saturate than and recovers faster than the gain, while the latter reason helps to produce high single-pulse energies. The four critical concepts which are used to generate these optical pulses can be summarized as follows: (1) A hybrid mode-locking technique is employed to provide both the advantages of the short-pulse forming mechanisms in passive mode locking, while maintaining the low timing jitter associated with active mode locking; (2) Angle-striped semiconductor traveling-wave optical amplifiers are utilized to eliminate undesirable reflections associated with imperfect anti-reflection coatings on the laser chip within the oscillator cavity; (3) The nonlinear dynamics are exploited to generate a wide bandwidth linearly chirped pulse, such that external dispersion compensation can compress the optical pulse; (4) Chirped pulse external amplification is used to reduce nonlinear gain saturation, which has the effect of maximizing the amplified optical pulse energy. These four concepts utilized together has allowed the production of optical pulses of 200 fs duration with over 165 W of peak power from a system using single-emitter injection-diode amplifiers.

The experimental arrangement utilized in these experiments is shown in Fig. 1. The external cavity mode-locked oscillator is constructed from a GaAs/AlGaAs angle striped SLA [16], a Multiple-Quantum-Well (MQW) saturable absorber which has been epitaxially removed from its substrate [17] and placed in contact with the rear reflector, a 50% output coupler, and a four-prism sequence which has been proven effective in reducing pulse length in many mode-locked laser systems. The prisms are composed of the glass type SF18 (index of refraction 1.72), with a prism separation of 33 cm. The MQW saturable absorber incorporates a modified design as compared to previous modelocking experiments [18]. This new design utilizes 7 wells of 6, 6.5, 7, 7.5, 8, 8.5, and 9 nm separated by 10 nm barriers. This stagger tuning creates an artificial inhomogeneously broadened absorption region thus creating the possibility for the support of a wider mode-locked spectrum or tunability. The absorption recovery time, measured by standard pump-probe techniques, was reduced to ≈150 ps by 200 keV proton implantation with a density of 10^{13} cm^{-2}. The absorber was annealed to eliminate aging effects. To illustrate the effect of combining several independent excitonic absorbers (Fig. 2a, b)

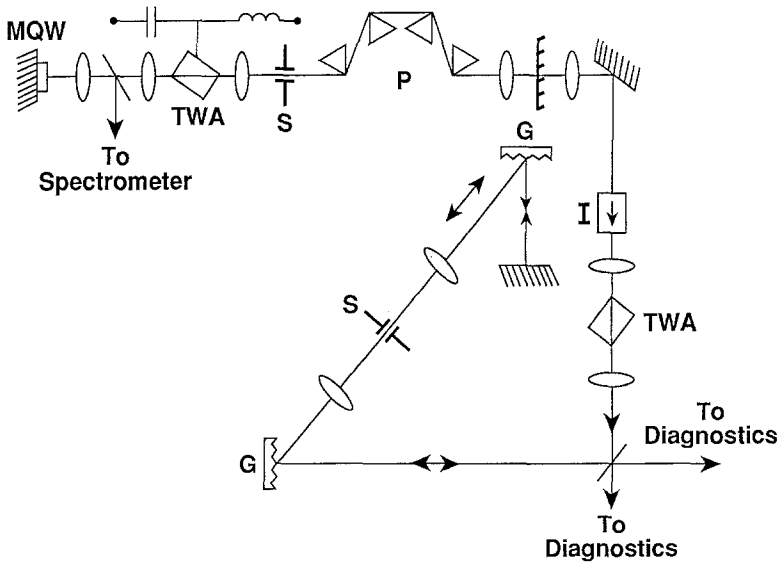

Fig. 1. Schematic of the external cavity semiconductor laser system. MQW broadband Multiple-Quantum-Well saturable absorber; S: Slit; G: Grating; I: Isolator; TWA: semiconductor Traveling Wave Optical Amplifier; P: Prism set

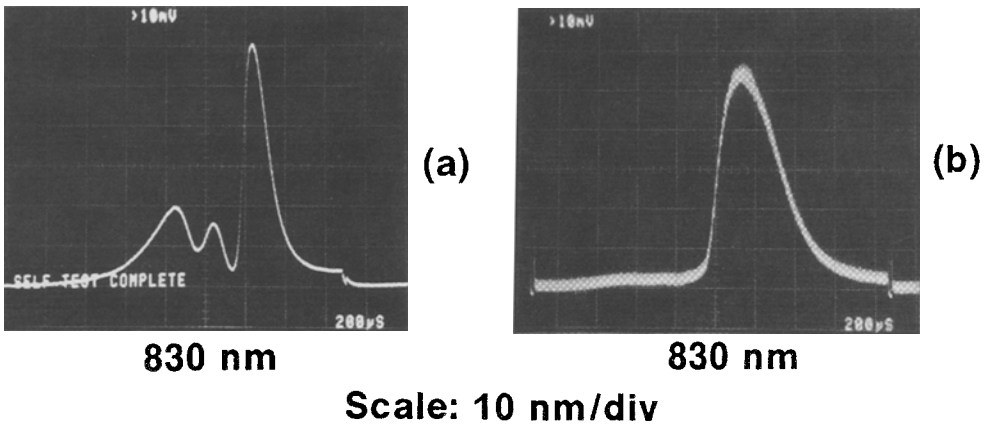

Fig. 2a, b. Transmission spectra of the MQW saturable absorbers using the spontaneous emission output of the TWA as a broadband source. **a** Conventional multiple quantum well absorber (quantum well width is equal to 70 Å) and **b** modified quantum well absorber, consisting of 70, 75, 80 Å wells. The excitonic absorption peaks evident in **a** are smeared out in **b**. The actual absorber used in the mode-locking experiments consisted of 7 wells in 5 Å steps from 60 Å to 90 Å

the transmission spectrum of a standard MQW saturable absorber is shown and compared to the transmission spectrum of the modified absorber used in these experiments. These data clearly show the differences between the spectrum of a single well and that obtained by "staggering" the well thickness. The external cavity has a fundamental longitudinal mode spacing of 111.8 MHz. The semiconductor optical amplifier chip is placed 15 cm from the rear reflector. Under passively modelocked operation, the laser oscillator operates at a repetition rate of 335.4 MHz, due to the 1/e gain recovery time of the amplifier (same as the carrier decay time τ_c) which we measured to be $\approx$1 ns. The pulse width in this case is approximately 5–7 ps with approximately 1 nm spectral width. The chirp is positive. In order to achieve hybrid mode-locked operation, an rf signal with $\approx$0.5 W of power is applied to the SLA through a bias-tee network. The rf frequency is chosen to match the third harmonic of the fundamental frequency, i.e. 335.4 MHz. The application of the rf drive signal serves to synchronize the laser and to broaden the passively mode-locked spectrum significantly, giving a lasing bandwidth of $\approx$7.2 nm, at a center wavelength of 838 nm. The optical pulses produced from the oscillator were highly chirped, with a pulse duration of $\approx$10 ps and a time bandwidth product of $\approx$30. These results were different from most ultrafast laser systems, since normally the function of the four-prism sequence is to balance the residual group-velocity dispersion and the resultant chirp impressed upon the pulse during the mode-locking process. Nonetheless, we find that the presence of the prisms as well as the stagger-tuned absorber is important. In the absence of either element additional spectral broadenening does not arise.

In order to obtain a better understanding of the mode-locking dynamics, intracavity spectra were measured at three important locations. These locations are (1) at the output coupler, (2) before the saturable absorber, and (3) after the saturable absorber. The results of these measurements are summarized in Fig. 3a–c. In Fig. 3b, the spectrum of the pulse is shown after exiting the gain medium, before the pulse enters the saturable absorber. The salient feature of this pulse spectrum is the predominant red peak, which is due to self-phase modulation resulting from rapid depletion of the gain [14, 19]. The measured gain experienced by the pulse is >30. In Fig. 3c, the pulse spectrum is shown after the pulse exits the MQW saturable absorber. A drastic modification of the optical pulse spectrum is observed, giving evidence that the optical nonlinearity associated with the saturable absorber is changing the optical pulse characteristics. The output spectrum, shown in Fig. 3a, is also modified with respect to the pulse spectrum shown in Fig. 3c. In this case, the reflected pulse enters the gain medium during a time when the gain is low. Because the gain medium is located close to the rear saturable absorber reflector, the gain does not have a sufficient time to recover completely. As a result, the gain medium is still saturated when the pulse is injected into the device. This is confirmed by observing that the gain experienced by the pulse is only $\approx$5. It should be noted that Group-Velocity Dispersion (GVD) in the laser diode should not play a major role in the spectral modification process for a bandwidth of 7 nm. Pulse broadening due to GVD is estimated to be only $\approx$200 fs, which is much less than the optical pulse duration within the cavity.

These results show that large changes in the pulsed optical field occur within one round trip. Conventional theories of mode-locking using quantum-well saturable absorbers show changes in the mode-locked pulse that are only of the order of a few percent [20]. We conclude that the hybrid mode-locking method used here imparts additional optical nonlinearities into the mode-locking process. The strong modifications in the spectral characteristics of the mode-locked optical pulse within one round trip also lead us to conclude that the nonlinearities experienced by an optical pulse in a hybrid mode-locked semiconductor laser are sufficiently large such that dispersion compensation with prisms provides insufficient compensation for the chirp induced by the gain dynamics. It may be noted that large changes in the pulse characteristics at different places in the cavity have also been observed in the mode-locked Ti : Saphire laser [21]. However, those changes can be understood as a discrete soliton formation process and are very different from the ones observed in our system. A detailed understanding of the nonlinear processes taking place in the amplifier is clearly very

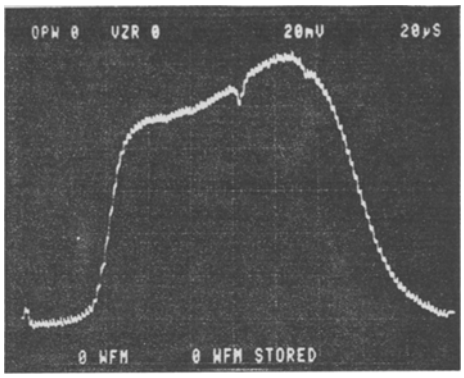

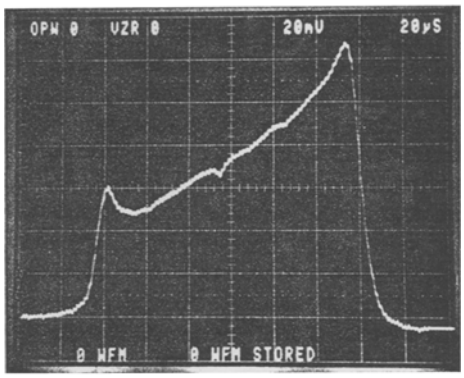

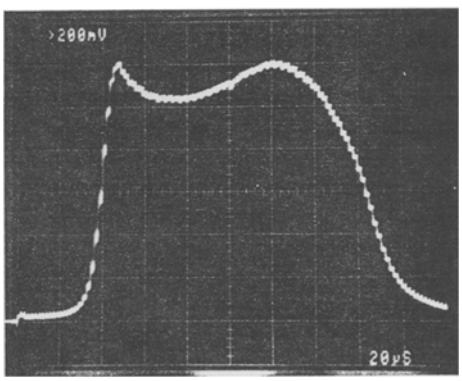

Fig. 3. Optical spectra at different locations in the cavity. *Top:* Output spectrum; *center:* spectrum after the gain medium; and *bottom:* Spectrum after the saturable absorber

important for a complete and satisfactory explanation of the mode-locking process.

Even though the intracavity prism sequence cannot compensate for the frequency sweep induced during the mode-locking process, it does play an important but not yet understood role. Without it, the perfectly coherent linear chirping of the pulse can not be achieved. With it in place, femtosecond optical pulses *can* be generated from this laser system. This is achieved by injecting the optical pulse train into a standard dual-grating compressor arranged in a double-pass geometry. This optical arrangement provides for a larger dispersion and thus can compensate the linear frequency sweep impressed on the optical pulse, resulting in the compression

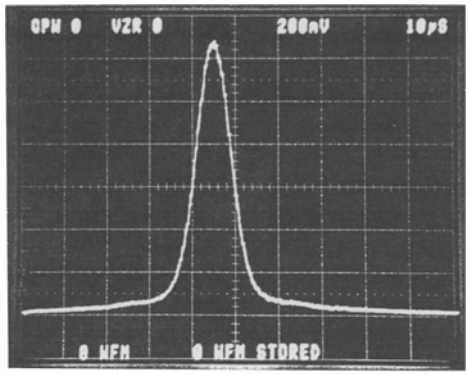

Fig. 4. Autocorrelation of the compressed pulse, showing a FWHM pulse duration of 207 fs, assuming a hyperbolic secant squared pulse profile. The average power after compression is 11.5 mW, implying a peak power of 165 W

of the pulse to nearly spectrally limited value, In the experimental configuration described above, the optical pulse is injected into another SLA prior to compression, in order to obtain high output power. The advantages of amplifying the optical pulse prior to compression is two-fold: (1) The effect of the pulsewidth-dependent gain saturation due to carrier heating and cooling [11, 14] is avoided, thus allowing for the generation of high output power optical pulses; (2) spectral filtering techniques can be employed in the Fourier plane of the compressor to eliminate the spontaneous emission from the amplifier, and thereby creating high contrast amplified pulses. It should be noted that the optical pulse shape and spectrum are negligibly affected by one external amplification stage. This is easily understood by noting that the injected optical power is less than the intracavity optical power. The spectral distortion is then inversely proportional to the pulse duration. For a 10 ps pulse, spectral distortion of the order of 0.05 nm may occur [14]. This will have little effect on the pulse shape, and has been confirmed by independent spectral and cross-correlation measurements of the pulse after amplification, as well as by the theoretical calculations presented in Sect. 3.

Experimentally, amplification of the hybrid mode-locked optical pulse train was accomplished by utilizing an SLA identical to the one used in the oscillator. With an injection power of 1–2 mW, amplified average output powers of over 30 mW were obtained, corresponding to around 80 pJ of energy per pulse. It should be noted that the injected optical power contained $\approx$75 μW of total background spontaneous emission distributed over the entire spectral output. The amplified pulse train was then injected into the dual grating compressor in a double-pass geometry. The compressed pulse was measured using a standard rotating-mirror autocorrelator. Figure 4 shows the compressed output of the amplified mode-locked optical pulse train generated from the hybrid mode-locked laser system. The autocorrelation trace shows an optical pulsewidth of 207 fs in duration, assuming a sech^2 pulse shape. The throughput power from the compressor yielded 11.5 mW of amplified output power corresponding to 34 pJ pulses, with less than 100 μW of background spontaneous emission, owing to the spectral fil-

ter. It should be noted that the presence of the MQW saturable absorber prevents any continuous lasing to occur, i.e., there is no cw component in the same spectral regime as the mode-locked optical pulse. Stable mode-locked operation over many hours, as indicated by continuous monitoring of the spectrum and the pulse train, is readily obtained. These results imply a peak power of 165 W, making these optical pulses both the shortest and most intense ever generated from an all-semiconductor diode-laser system. A second stage amplification results in strong spectral distortions for both compressed or uncompressed pulses, as well as in some changes of the pulse shape. We performed a series of such experiments for the purpose of investigating the nonlinear processes occuring in the SLA. The results of these experiments are described in Sect. 3 where we compare them with the predictions of our new theoretical model.

In summary, in this section we described hybrid mode locking of an external cavity semiconductor-laser system with the inclusion of a four-prism sequence and a new design of a MQW saturable absorber that has resulted in the generation of optical pulses of 207 fs in duration with over 160 W of peak power. The intracavity spectra have also been measured in this laser system. The results show that spectral reshaping mechanisms associated with gain depletion and saturable absorption are so large that a standard four-prism sequence does not provide adequate compensation to directly produce transform-limited optical pulses directly from this type of laser oscillator. Alternative methods for intracavity compensation of frequency chirp which provide larger dispersion, such as grating compensators, may prove fruitful for accomplishing this task. However, the detrimental effects of the pulsewidth-dependent gain saturation must be avoided if high output peak powers are desired.

2 Theoretical Model for Pulse Amplification in an SLA

We present here an improved and more general version of our theoretical model [22, 23] for femtosecond-pulse single-pass amplification in an SLA. The propagation of the pulse in the SLA is described by a nonlinear equation for the complex time-domain pulse envelope. Thus, not only intensity but phase-shaping effects are modeled. Most importantly, the equation includes the rapid gain *and* phase dynamics which have been observed through pump-probe experiments [8–14] and have been attributed to carrier heating and subsequent cooling. Although essentially phenomenological, this equation is nevertheless firmly rooted in the underlying device physics. It can be obtained by a spectral domain expansion [22] of the complex susceptibility owing to the injected carriers and to the background material. The carrier-induced susceptibility is a function of both the carrier density and the carrier temperature which in turn are changed by the interaction with the amplified pulse. These dynamics are described by additional equations which were obtained using simple models [8, 19, 22, 24] and the rate equation approximation (equivalent to adiabatic elimination of the polarization). It is well known that this approximation becomes invalid when the pulse duration approaches the polarization-dephasing and intraband-relaxation times. The actual values fo these time constants are not known but are thought variously to be as long as ≈200 fs or as short as ≈30 fs. Our approach is to assume that rate equation approximations *can* be used for pulses even in the subpicosecond range. The limits of validity should be decided by comparison of the results obtained from our model with experimental measurements.

The nonlinear propagation equation is given below without derivation, but with physical explanation of its various terms and comparison with previous models [19, 25]. Following previous models, the transverse dependence of the pulse (assumed constant in the amplifier) has been integrated out and appears only through an effective area $A = wd/\Gamma$ (wd is the cross section of the active region and Γ is the confinement factor defined in the standard manner). The complex pulse envelope $V(\tau, z)$ (defined so that $|V(\tau, z)|^2$ has units of power), which includes all the phase effects except the carrier propagation, evolves with propagation distance z and local time $\tau = t - z/v_g$ according to

$$\begin{aligned}
&\left[\frac{\partial}{\partial z} - \frac{\mathrm{i}}{2}\beta_2\frac{\partial^2}{\partial\tau^2} + \frac{\gamma}{2}\right.\\
&\quad\left. + \left(\frac{\gamma_{2\mathrm{p}}}{2A} + \mathrm{i}\frac{\omega_0}{cA}n_2\right)|V(\tau,z)|^2\right]V(\tau,z)\\
&= \left[\frac{1}{2}g_{\mathrm{N}}(\tau,\omega_0)\left(\frac{1}{f(\tau)} + \mathrm{i}\alpha_{\mathrm{N}}\right) + \frac{1}{2}\Delta g_{\mathrm{T}}(\tau,\omega_0)(1+\mathrm{i}\alpha_{\mathrm{T}})\right.\\
&\quad - \left(\frac{\partial\zeta(\tau,\omega)}{\partial\omega} + \frac{\mathrm{i}}{2}\frac{\partial g(\tau,\omega)}{\partial\omega}\right)_{\omega_0}\frac{\partial}{\partial\tau}\\
&\quad\left. + \left(\frac{\mathrm{i}}{2}\frac{\partial^2\zeta(\tau,\omega)}{\partial\omega^2} - \frac{1}{4}\frac{\partial^2 g(\tau,\omega)}{\partial\omega^2}\right)_{\omega_0}\frac{\partial^2}{\partial\tau^2}\right]V(\tau,z)\,. \quad (1)
\end{aligned}$$

The first line of (1) is recognized as the well-known nonlinear Schrödinger equation used to describe pulse propagation in passive third-order nonlinear media, with the minor modification that a linear loss γ and Two-Photon Absorption (TPA), $\gamma_{2\mathrm{p}}$, have been added. Thus, β_2 is the GVD coefficient due to the background (material and mode) index and $\omega_0 n_2/cA$ is the SPM term due to the instantaneous nonlinear index n_2. The juxtaposition of $\gamma_{2\mathrm{p}}/2A$ and $\omega_0 n_2/cA$ indicates the fact that n_2 is in part due to the dispersion of TPA [27].

The second line of (1) has two groups of terms which together account for the carrier density (N) induced nonlinear gain dynamics at the pulse center frequency ω_0 and for the associated Self-Phase Modulation (SPM). The gain is reduced by carrier depletion and by carrier heating. Since the pulse is much shorter than the carrier lifetime τ_{c}, the saturation of the gain due to carrier depletion is given by the well-known expression [19]

$$g_{\mathrm{N}}(\tau) = g_0\exp\left(-\frac{1}{W_{\mathrm{s}}}\int_{-\infty}^{\tau}|V(s)|^2\mathrm{d}s\right), \quad (2)$$

where g_0 is the linear gain and $W_{\mathrm{s}} = \hbar\omega_0 A/a_{\mathrm{N}}$ is the saturation energy (a_{N} is the phenomenological gain coefficient). The function $f(\tau)$, which does not appear in our earlier reported work [22, 23], accounts for a hole-burning gain reduction which is assumed to have a response time of τ_{i}, the intraband thermalization time:

$$f(\tau) = 1 + \frac{1}{P_{\mathrm{sh}}\tau_{\mathrm{i}}}\int_{-\infty}^{+\infty}u(s)\mathrm{e}^{-s/\tau_{\mathrm{i}}}|V(\tau-s)|^2\mathrm{d}s\,, \quad (3)$$

where P_{sh} is the hole-burning saturation power. For $\tau_i \to 0$, $f(\tau) = (1 + P(\tau)/P_{sh})$, an instantaneous saturation. No contribution to the index by the hole-burning is included, however. This approximation is based on the fact that the real part of the susceptibility is owed mostly to the large absorption at energies well above the bandgap. Thus, to first order, a broad hole in the gain will have only a small effect on the index. For pulse widths longer than τ_i this contribution to the index will follow the pulse intensity envelope and can be incorporated in the effective n_2.

We model the additional gain reduction caused by the carrier heating effect by the equation

$$\Delta g_T(\tau) = -\int_{-\infty}^{+\infty} u(s)\,(1 - e^{-s/\tau_i})\,e^{-s/\tau_2} \times [h_1|V(\tau - s)|^2 + h_2|V(\tau - s)|^4]\,ds\,. \quad (4)$$

Here, $u(s)$ is the unit step function, and τ_2 is the relaxation time of the heated carrier temperature (T) back to ambient lattice temperature (T_L) due to carrier-phonon scattering. The heating of the carriers is assumed to owe to three processes which either remove low-energy ("cool") carriers or add high-energy ("hot") carriers. The constant h_1 describes the contribution of Stimulated Emission (SE) and Free-Carrier Absorption (FCA) to the carrier heating gain reduction, and h_2 describes the contribution of TPA. This contribution depends on the fourth power of the pulse amplitude (power squared), because the carrier temperature rise is proportional to the energy added to the conduction band via TPA. It is evident that the above three processes have indirect effects on the gain via the carrier heating, separate and distinct from their direct effects. If the magnitude of these processes are known, then the coefficient h_1 and h_2 can be estimated by calculating the energy change of the carrier gas during the passage of the pulse and recalculating the gain at the resultant higher temperature [25]. It should be noted that TPA adds carriers to the conduction band. Therefore, it would seem that a gain-*increase* term also ought to be present. However, by approximate calculations of both carrier temperature and carrier density increases and of the corresponding gain changes [22], we have shown that, at least for the range of values relevant to this paper, the gain increase owed to the added carriers is smaller than the gain decrease owed to the carrier heating and can be neglected. We also include a time delay for the onset of the higher carrier temperature. For our model, in agreement with recent experimental results [13], this is taken to be the same as the intraband thermalization time τ_i.

The SPM associated with the gain dynamics is described by the two Linewidth Enhancement Factors (LEF)

$$\alpha_N = -\frac{\partial\chi_R/\partial N}{\partial\chi_I/\partial N}\,, \quad (5)$$

$$\alpha_T = -\frac{\partial\chi_R/\partial T}{\partial\chi_I/\partial T}\,. \quad (6)$$

These are assumed to be constants for a particular value of carrier injection in a particular device. This approximation is good only if ΔN, the change in carrier density during saturation, is small compared to the unsaturated value N_{ss}. This may not always be true for high gain, strongly saturated amplifiers. Thus, the two LEF may in fact vary some during the pulse. We do not, for now, attempt to account for these effects or for variations that may originate from coherent effects which gradually come into play as the pulse width becomes comparable to τ [27]. As will be seen in the next section, this approximation does not negatively impact the ability of the theory to quantitatively explain the experimental results.

The third line of (1) contains the terms which describe the dynamic dispersion (frequency dependence) of the carrier-induced gain and index to second order. If the coefficients are constant in time τ they are straightforward to understand. The gain dispersion shifts and bandwidth limits the pulse spectrum. The index dispersion terms

$$\left[\frac{\partial\zeta(\tau,\omega)}{\partial\omega}\right]_{\omega_0}\frac{\partial}{\partial\tau}$$

and

$$\left[\frac{i}{2}\,\frac{\partial^2\zeta(\tau,\omega)}{\partial\omega^2}\right]_{\omega_0}\frac{\partial^2}{\partial\tau^2}$$

are simply corrections on the groups velocity and on GCD, respectively, and can be included in them. Owing to carrier depletion and to carrier heating, however, the frequency derivatives may be time-dependent quantities and their effect on the pulse can be more complex. In our earlier reported work [22] we have shown that in some SLAs (e.g. GaAs) carrier-induced index dispersion is negligible to a good approximation. Here, we have included the dispersion of the carrier-induced index in the propagation equation for the sake of completeness, and also because recent calculations indicate that in quaternary compound SLAs it may be not entirely negligible. We have also shown [22, 23] that, except for photon energies very close to the bandgap, the dynamic gain dispersion can be modeled by simple linear dependences on the instantaneous gain (without the hole-burning correction), i.e. on $g(\tau,\omega_0) = g_N(\tau,\omega_0) + \Delta g_T(\tau,\omega_0)$,

$$\left.\frac{\partial g(\tau,\omega)}{\partial\omega}\right|_{\omega_0} = a_1 + b_1[g_0 - g(\tau,\omega_0)]\,, \quad (7)$$

$$\left.\frac{\partial^2 g(\tau,\omega)}{\partial\omega^2}\right|_{\omega_0} = a_2 + b_2[g_0 - g(\tau,\omega_0)]\,. \quad (8)$$

Here a_1 and a_2 are, respectively, the slope and the curvature of the linear gain (at the pulse center ω_0), while b_1 and b_2 are constants describing changes in these quantities with saturation. These changes occur because saturation alters the shape of the gain spectrum. The value of these constants may be estimated from the simple model calculation of the susceptibility [22] or from experimental measurements of the gain versus frequency curve.

Equation (1), together with the auxiliary equations (2–8) describe the propagation of the pulse in the SLA. Each of its terms derives from easily understood underlying physical effects. In principle, it is possible to calculate all the relevant parameters, or at the least, the path toward estimating them is clear. In practice, exact calculations are impractical due to inadequate knowledge of the details of the physics

and because many of the parameters are device-geometry dependent as well. In this work we treat the equations as essentially phenomenological and determine the parameters either from previous experimental investigations (e.g. pump and probe measurements) or from fitting to the results of actual amplification experiments. In the next section we apply the theory to our SLA devices in the subpicosecond regime.

3 Comparison of the Theory with Experiments

The pulse amplification experiments were carrier out on the same devices that were used in the hybrid mode-locked laser oscillator described in Sect. 1. The approximately 2–3 pJ uncompressed picosecond pulses from the laser oscillator could be amplified to ≈80 pJ in the nearly linear amplification regime with only small pulse shape or spectral distortions. However, when amplified in another stage, strong spectral distortions became evident, whether uncompressed, partially compressed or optimall compressed pulses were used as the input. It was found that the exact form of the spectral distortions was a very strong function of the time-domain pulse length. Although less dramatically evident, and difficult to diagnose quantitatively, some time-domain pulse distortions were also present. These effects are owing to the combined action of the various nonlinear processes in the amplifier as well as to the dynamic dispersion of the gain.

We test the theory in the subpicosecond regime by applying it with the *same* set of parameters to the results of two different sets of experiments. The first experiment was the measurement of the input and output spectra of the amplifier operating with a measured linear gain of 19 dB to 20 dB, using as actual input signal (after coupling in losses) ≈7 pJ pulses of ~460 fs and 2 ps durations. Both of these inputs were obtained from the output of the compressor after chirped pulse amplification and had identical spectra. The longer pulses were obtained by nonideal compression in the compressor stage which effectively added a linear chirp. The second experimental involved measuring the time resolved gain for each of the above two inputs by a standard pump-probe technique, using the same pulse for the pump and the probe in each case. The equations of the theoretical model were numerically integrated from $z = 0$ to $z = L$ using a modified split-step Fourier-transform method which gave the pulse evolution versus propagation distance z in both time and frequency domains. In our calculations, we use 2048 for both the number of spatial and temporal segments. The accuracy of this numerical method has been tested by comparing the results (output pulse shape, spectrum and output pulse energy) after doubling the number of spatial and temporal segments. The comparison reveals insignificant differences in single precision for the range of parameters that we explore in this paper. The computer that we use is a HP 9000/710 workstation. The CPU execution time for calculating these results is approximate 9 min. The equations contain a large number of parameters, very few of which are accurately known. We varied them through a range of values, either obtained approximately from our experiments [2, 23] or suggested by published theoretical [25, 28] or experimental [9, 10, 13, 29] data, until a good fit with *both* sets of experiments was obtained. The final set of parameters are listed in Table 1 and they will be discussed further below. We found that the results were quite sensitive to most of the parameters of the equations and very sensitive to the input pulse shape, especially asymmetry. Therefore, we fashioned a subpicosecond theoretical input pulse by a combination of time- and spectral-domain shaping which gave a spectrum very closely corresponding to the experimentally measured one. Since the experimental pulse was approximately spectrally limited, we assume zero spectral phase, Without this process of approximation of the actual input pulse it was impossible to match the experimental results.

Table 1.

Parameter	Value	Units
W_{in}	7.1	pJ [a]
A	5.0	μm
L	500	μm
γ	23	cm^{-1} [b]
β_2	0.05	ps^2/cm
γ_{2p}	0.055	cm/MW
n_2	− 0.64	cm^2/TW
g_0	111	cm^{-1} [c]
W_s	69	pJ
P_{sh}	31	W
h_1	0.13	$cm^{-1}\,pJ^{-1}$
h_2	126	$s\,cm^{-1}\,pJ^{-2}$
α_N	3.1	
α_T	2.0	
τ_2	700	fs
τ_i	60	fs
a_1	0.15	fs/μm
b_1	− 80	fs
a_2	− 60	$fs^2/\mu m$
b_2	0	fs^2

[a] Experimental value, assuming 52% input loss
[b] Linear loss $L_0 = \exp(\gamma L) = 5$ dB
[c] Linear gain $G_0 = \exp(g_0 L) = 24$ dB

The theoretical time-domain pulse shapes are shown in Fig. 5. The bandwidth-limited pulse (Fig. 6a, solid line) is 430 fs long with $\Delta t \Delta f = 0.53$. (It is 0.58 in the experiment if a $sech^2$ pulse shape is assumed which is, of course, only an approximation.) The longer pulse (Fig. 5b, solid line) was derived from the above in the same manner as was done experimentally, i.e. by adding a sufficiently large quadratic phase to the spectrum (linear carrier chirp) to broaden time duration to ≈2 ps. The dashed curves are the calculated output pulses. For the shorter pulse the most important feature is that the subsidiary peaks on the front are strongly accentuated during amplification. Since the pulse shapes were not diagnosed, no detailed comparison with the experiment could be made. However, autocorrelation measurements of the output signal showed a pedestal broadening consistent with the calculated pulse shape.

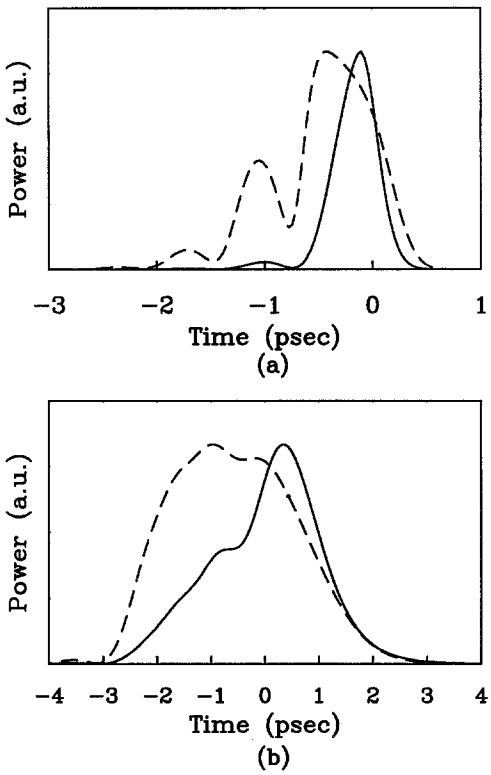

Fig. 5a, b. Theoretical input and output pulse shapes for the single-beam amplification experiments. *Solid lines* are input pulses fashioned by time- and spectral-domain shaping. *Dashed lines* are output pulses calculated using (1–8) and the parameters of Table 1 for: **a** spectrally limited 430 fs input pulse, which spectrum as given in Figs. 6a, **b** 2 ps input pulse with the same spectrum

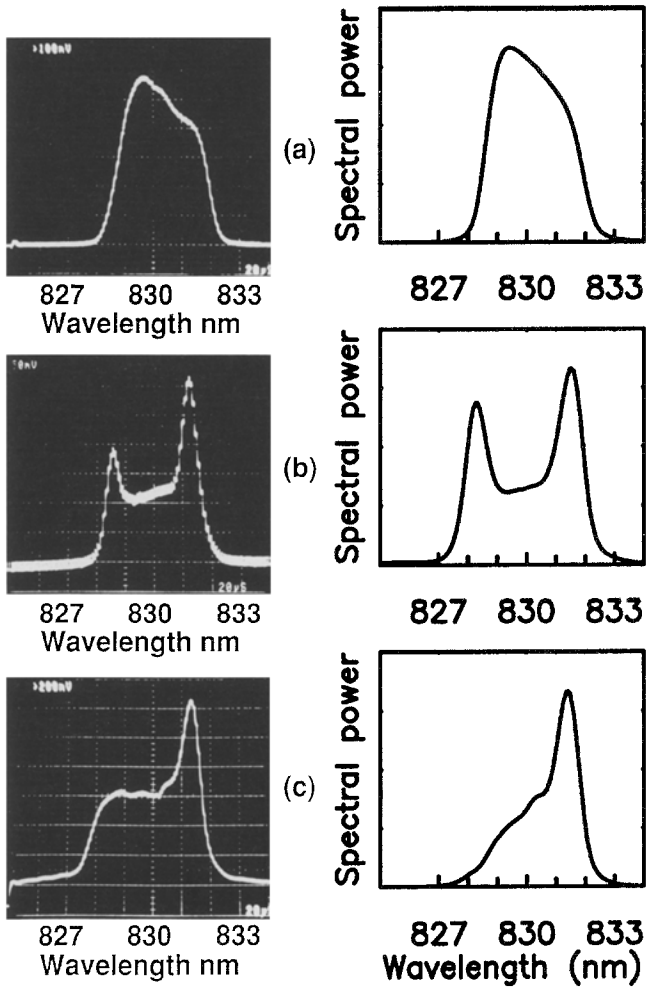

Fig. 6a–c. Comparison of experimental and theoretical spectra for the amplification experiment. The theoretical spectra were calculated for the pulses shown in Fig. 5. **a** Input spectrum; **b** output spectrum for the subpicosecond pulses; **c** output spectrum for the 2 ps pulses

Figure 6 shows quantitative comparison of the experimental and theoretical spectra for the first experiment described above. Very good agreement can be seen, with all the salient features of the measured output spectra duplicated in the theoretically calculated ones. Especially noteworthy is the excellent reproduction of the two peaks with a flat sloping region in between, for the 460 fs pulse case. For the longer pulse the agreement is also satisfactory. The most important feature of the experimental curve, i.e. the total abscence of the short-wavelength peak, is again reproduced. The main difference is a somewhat less pronounced short-wavelength should on the theoretical curves. We also calculated pulse evolution (not shown) for 10 ps duration pulses, corresponding to amplification of the uncompressed pulses. With the same input pulse energy of $W_{\text{in}} = 7.1$ pJ, the net (saturated) gain calculated for the three cases was 3.6, 7.0, and 12.1 for the 430 fs, 2 ps and 10 ps pulses, respectively. These are also in good agreement with the experiments, although the comparison is only approximate since the insertion losses were not accurately known. It was also verified that when 10 ps uncompressed pulses of $\approx$2 pJ energy are used as the input, as in the amplification preceding the compressor described in Sect. 1, there is negligible temporal and only small spectral distortion present.

Figure 7 shows comparison of the experimental and theoretical results for the pump and probe experiments, using the same parameters in the equations as for the single beam experiments. The theoretical results were obtained by calculating the cumulative time-dependent gain and then convolving it with the input pulse. In Fig. 7a, with the 430 fs pulse as pump and probe, two different gain-reduction mechanisms are prominent, in agreement with the experimental results. The fast recovering one is attributable to the carrier-heating effect, while the step-like portion (whose recovery is not shown because it is on a much longer time scale) is owing to the carrier depletion. The proportions of the two saturations and the recovery time of the carrier heating are also correct. For the 2 ps pulse case the fast recovering-gain depletion is almost completely absent in the experiment. It is notable that this happens for a factor of only about four increase in the pulse duration. This strongly suggests that a higher than linear-order process is mainly responsible for the heating of the carriers. Indeed, the theory could be matched to both the long- and short-pulse pump-probe results only if the two parameters which control the magnitude of the carrier-heating gain reduction (h_1, h_2) were adjusted in such a way that the second (intensity squared) term in (3) dominated over the one proportional to the intensity. We tentatively interpret this to mean that the carrier heating in this device is mainly due to TPA rather than to FCA or SE.

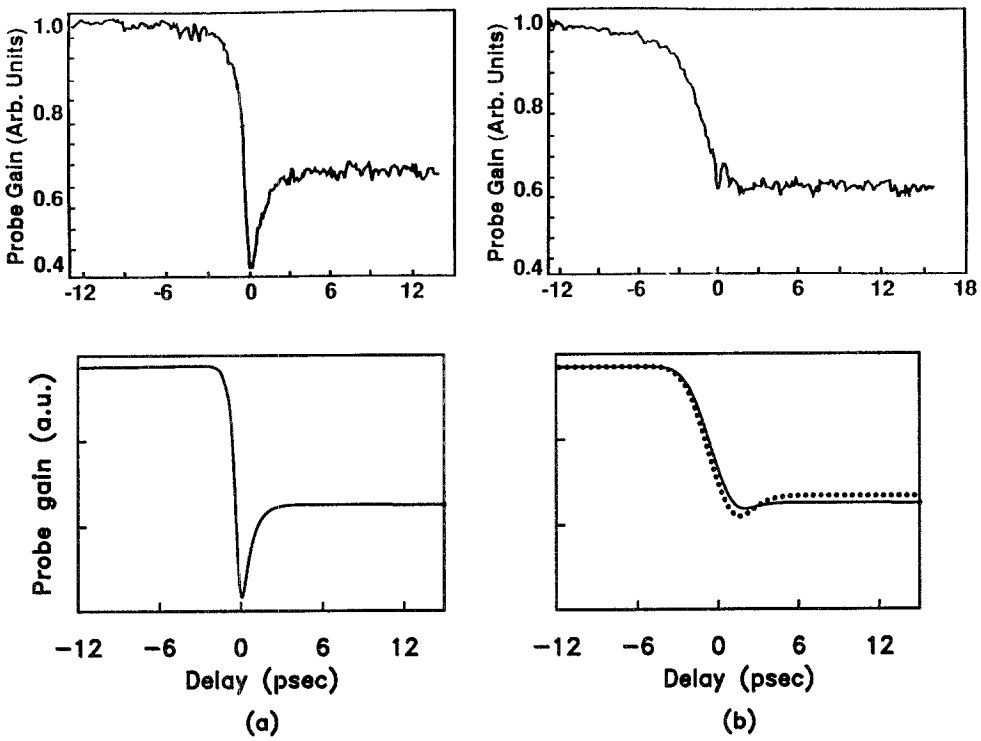

Fig. 7a, b. Comparison of experimental and theoretical results for the pump-probe experiments. **a** Using the 430 fs pulses as both pump and probe, **b** using the 2 ps pulses as both pump and probe. For the theoretical curves (*lower panel*), *solid line* is with parameters as given in Table 1, the contribution of h_2 predominates the carrier-heating gain reduction; *dotted line* is for $h_1 = 2.6\,\mathrm{cm}^{-1}\,\mathrm{pJ}^{-1}$, $h_2 = 0$. In **a** *solid* and *dotted lines* are indistinguishable

The spectral distortions were found to be rather sensitiviely dependent on nearly all the parameters of the equations and on the input pulse parameters (especially the shape). This was less so for the time-domain distortions. The important implication for experimental investigations is that spectral-domain experiments, in addition to time-domain pump-probe ones, are needed for a full diagnosis of these devices. It is instructive to explore in some detail the roles, the relative importance and the interactions of the various time- and frequency-domain amplitude- and phase-shaping effects during the pulse evolution in both domains. We gave some results of such explorations in our earlier reported work [23]. For example, it was shown that the characteristic blue peak and the flat region in the output spectrum of the subpicosecond pulse are the result of a complicated addition of the three kinds of SPMs, and of the influence of the pulse-shape changes. In particular, SPM due to the instantaneous nonlinear index n_2 and to the carrier heating play equally important roles. Here, we want to further discuss the implications of some of our theoretical parameters, focusing on the ones which were knewly added, and on the differences introduced by these modifications of the model. It must be noted that, due to the large number of parameters, it is not possible to say that a unique and truly optimized fit has been found and that the set of parameters given in Table 1 are accurate values for our device and its materials. Moreover, all of them are spatial averages, some over the gain region only, others over both the gain and the transparent cladding regions. Nevertheless, if our theory is to be a generally applicable one, the parameters should fall within reasonable bounds. It is very encouraging that this is, in fact, the case.

One of the important physical characteristics which determine the behavior of this SLA is that the frequency dispersion of the carrier-induced refractive index (as calculated [22] by a simple but reasonable model using an ensemble of Lorentzian lines and quasi-fermi statistics) is an essentially linear dependence with a slope nearly independent of carrier density and temperature. Physically, this is because the real part of the susceptibility is owed mainly to the large absorption at energies well above the bandgap. Because of this fact, in what follows, the two index dispersion parameters $[\partial\zeta(\tau,\omega)/\partial\omega]_{\omega_0}$ and $[\partial^2\zeta(\tau,\omega)/\partial\omega^2]_{\omega_0}$ are set to zero, the former being included in the effective group velocity and the latter neglected. Thus, GVD is owed to the background only and is very small, as confirmed in pump-probe experiments [9] by other groups. The large-signal behavior of the SLA is strongly influenced by this fact. The small β_2 has negligible effect on pulse evolution and consequently the nonlinear frequency chirps induced by the three different SPMs have a much weaker influence on the time-domain pulse evolution than is found in systems with significant GVD (e.g. soliton formation). This allows us to examine the time domain saturation effects (and the pump-probe results) independently from the frequency-domain distortions.

The decreasing value of the net gain with decreasing pulse width has been previously observed [11] and also theoretically examined [25]. It is attributable to the increasing effect of the carrier heating, which is completely negligible for the 10 ps (uncompressed) input pulse, very small for the 2 ps input pulse, and very important for the 430 fs one. The hole-burning saturation acts as an essentially instantaneous gain reduction for all three cases, because its time constant

(τ_i) is much shorter than all the pulse durations. (Our value for this time constant is not arbitrary, it will be discussed further below.) For the uncompressed pulse, gain saturation is determined by the carrier depletion and to a lesser extent by hole-burning. Thus, very similar results can be obtained using the theory established for long (≈10–100 ps) pulses [19]. The carrier depletion saturation parameter W_s is large (69 pJ) for this SLA. This is owed to the very thin gain region and resultant small confinement factor, and allows amplification of the stretched pulses to record high energies [2]. For the shorter pulses, the gain reduction caused by the carrier heating comes into play. This is governed in our equations by the two constants h_1 and h_2, reflecting the contributions of the linear (SE and FCA) and nonlinear (TPA) effects to the carrier temperature rise. As was already noted, and can be seen from Fig. 7, the pump-probe results could be matched only if the nonlinear contribution due to TPA dominates. The actual value of h_2 used for the matching is physically realistic as was determined by comparison with theoretical calculations [25] and by estimates corresponding to our experiment. It must be pointed out, that further experiments on this and other amplifiers with different materials and geometries should be carried out before definitive conclusions can be drawn regarding this result.

As to the hole-burning saturation, we note that in our earlier reported work [23] it was possible to match the experimental results quite well without including it in the model. We have now added it to the theory for two reasons. First, results of recent pump-probe experiments [13] as well as comparison with theory [15] strongly suggest that hole-burning *is* present and plays a partial role in the gain saturation. Second, its inclusion allows us to use a higher net small-signal gain in all the theoretical calculations, a value which is now in excellent agreement with the experimentally measured ≈19 dB to 20 dB. (Note that from Table 1, $G_{0(\text{net})} = G_0 - L_0 = 24 - 5 = 19$ dB.) Without the hole-burning saturation a linear gain of 22 dB had to be used [23] corresponding to $G_{0(\text{net})} = 17$ dB. The hole-burning saturation power P_{sh} determines the amount of gain reduction caused by this effect. Its value of 31 W is large, resulting in a relatively weak hole-burning saturation even for these strongly amplified pulses. Like the large W_s, physically this too owes to the very thin gain region of our device. Equations (3) and (4), which describe hole-burning and carrier-heating gain reductions, respectively, also contain two time constants: τ_2, the decay rate of the heated carrier temperature and τ_i, the intraband relaxation time which appears as the hole-burning time response and also as a delay in the establishment of the carrier temperature rise and of the resultant gain reduction. The value of τ_2 was determined by the decay of the fast gain reduction in the subpicosecond pump-probe results (Fig. 7a) and is consistent also with measurements by the MIT group [9, 10]. By contrast, τ_i is certainly shorter than our shortest pulse and is therefore not directly manifested in the pump-probe results. It does, however, have indirect effects on both the gain saturation and on the spectral distortions. Variations of its value between 25 fs and 200 fs only very weakly affected the time domain results and our value of 60 fs was determined mainly by fitting the spectral domain distortions as discussed in the next paragraph. It is important to note that, although we found it convenient above to discuss several of the parameters in terms of the time-domain effects, all of them (except β_2) have strong influences on the frequency-domain results. Additionally, while the time-domain evolution is only very weakly dependent on the spectral changes, the spectral distortions are very strongly affected by the pulse-shape changes. This sensitivity of the output spectrum allowed not only a "fine tuning" of the parameters already discussed above, but also the determination of the ones which do not influence the pulse shape.

The spectral distortions are determined primarily by the combination of three nonlinear chirps by three SPMs: those owing to the carrier density and temperature changes and that owing to the instantaneous nonlinear index n_2. The fitting values for the two LEFs (which control the first two SPMs) are reasonable for this SLA and the value of n_2 is in excellent agreement with recent experimental measurements [29]. As was mentioned above, the intraband relaxation time τ_i also influences the spectral distortions, and does so mainly through the delay in the carrier-heating SPM. This important physical parameter is very little known and is difficult to measure. Recently, a value of $\approx 120 \pm 60$ fs was determined by pump-probe experiments [13] but the possible error was large. Another, indirect measurement [30] gave a value of 50 fs. We arrived at our estimated value of 60 fs in the following manner. For values of τ_i ranging from 25 fs to 200 fs, we were able to fit quite well both the spectral distortions (Fig. 6) and the pump-probe results (Fig. 7), with readjustments of certain other parameters. The best fit, however, was obtained for $\tau_i \approx 60$ fs. Moreover, increasing τ_i beyond ≈100 fs necessitated a considerable increase of the LEF α_N. For example, for $\tau_i = 180$ fs, $\alpha_N = 5.1$ was required, which is an unreasonably large value for GaAs devices. On the basis of these series of results, we may state that τ_i appears to be shorter than 100 fs and we use 60 fs as the most likely value.

Given the remarkable success of the theory in explaining the experimental results, it can be confidently concluded that it is indeed valid for pulses in the subpicosecond regime and that, even for pulses as short as ≈400 fs, a full coherent Bloch-Maxwell analysis [27] is not needed. It is, of course, likely that at these pulse durations some coherent effects do begin to appear. What our results indicate is that these effects are relatively weak and are not a major factor in the behavior of the SLA. We attempted to further explore this point by modifying our equations to reflect a prediction of a recent theory based on such an approach [27]. It was predicted that for pulses of ≈0.5 ps duration the linewidth enhancement factor α_N is a time-dependent quantity. We have incorporated the predicted time dependence in our theory by approximating it with an algebraic function. This did result in some changes in the sensitively dependent calculated output spectrum. By readjusting some of the parameters we were still able to match the experimental results. To this point, however, we have not obtained any improvement in the agreement. We also note that the assumptions on which our phenomenological model is based are equivalent to those made in the recent paper of mark and Mørk [15] whos have obtained excellent agreement with the results of gain and loss pump-probe experiments using 150 fs pulses.

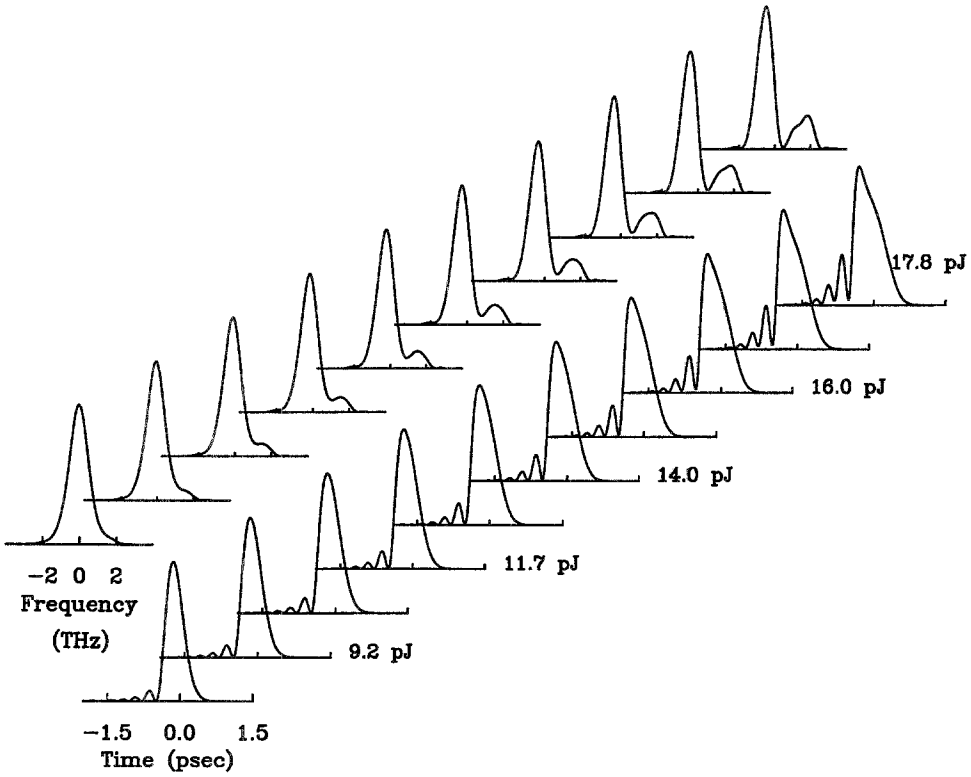

Fig. 8. Calculated evolution of the pulse spectrum and the pulse intensity in the amplifier for a 250 fs input pulse which was broadened by third-order dispersion-time advances

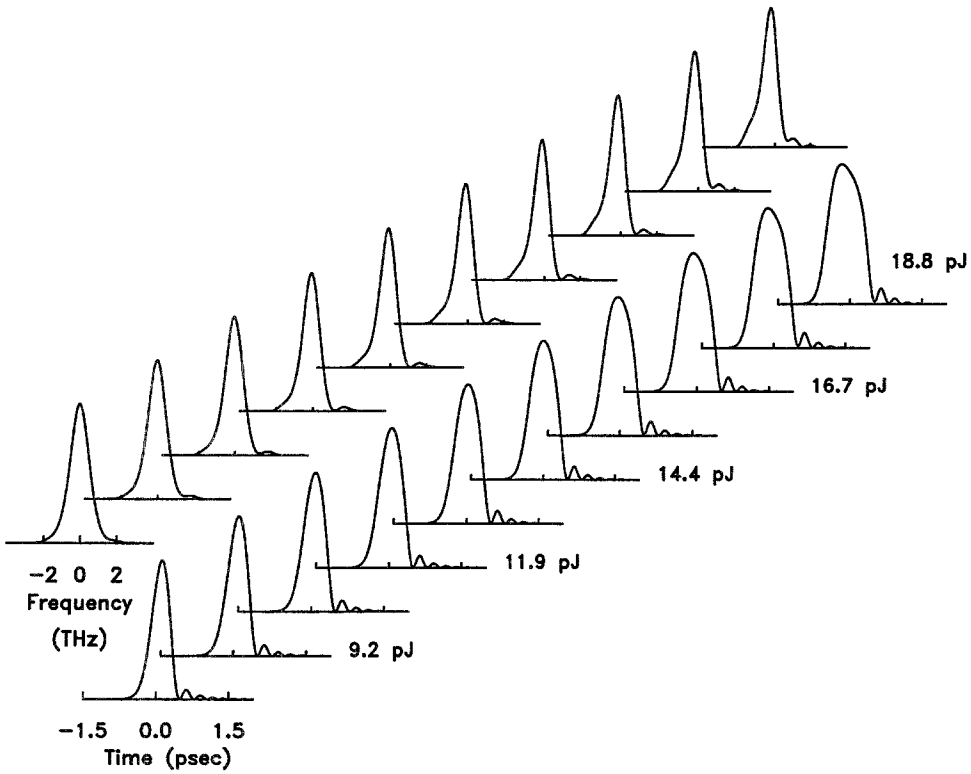

Fig. 9. Calculated evolution of the pulse spectrum and the pulse intensity in the amplifier for a 250 fs input pulse which was broadened by third-order dispersion-time delays

To investigate the limits of validity of our theory further experiments with controlled-shape input pulses are needed. Such experiments are currently in preparation in our laboratory. In Figs. 8 and 9 we show the predictions of the model for a set of experimentally realizable pulses which are somewhat shorter than the ones used above. The two different asymmetric pulses were obtained from bandwidth-limited, symmetric, sech^2-shaped, 250 fs pulses by adding a certain amount of third-order dispersion with both possible signs. The resultant pulses are only very slightly broader but have subsidiary peaks on either the leading or on the trailing edge. These pulses can be made with relative ease and good accuracy utilizing the Heritage-Weiner frequency-domain pulse shaper combined with a cubically distorted mirror [31]. The predicted pulse evolutions, are shown versus distance in the amplifier in both temporal and spectral domains. The spectral evolution is dramatically different for the two cases. For both cases there is a red-shifted peak consolidating out of the

red side of the input spectrum. Additionally, the input pulse with the temporal interference preceeding the main pulse shows the evolution of a distinct and separate blue peak. When the pulse is flipped in time this blue peak is nearly totally absent. The blue peak owes mainly to the influence of a negative nonlinear index and to the rapid temporal rise in pulse intensity caused by the major interference dip. For the case when the interference dip is on the trailing edge, the SPM contributes to the red shift instead. We note also that for these shorter pulse durations both the carrier depletion and the carrier heating act as integrating saturations. Consequently, further reduction of the pulse width (we calculated cases down to 150 fs) did not result in any significant changes in the type of distortions predicted by this model, in contrast with the dramatic changes predicted (and verified) when the input pulse duration was changed from longer than the carrier colling time constant (τ_2) to a shorter value. Comparison of these and similar predictions with experiments should further advance the understanding of the model and help to clarify its limits of validity. In particular, we note that index contribution owing to spectral hole-burning will change from essentially instantaneous to integrating type as the pulse widht is reduced below $\approx$200 fs, and can no longer be incluced in n_2. Future experiments with such and even shorter pulses will help to clarify how to include these effects as well as those due to coherent interactions in the model.

4 Summary and Conclusions

We presented in this paper results describing the utilization of our semiconductor optical amplifiers for the generation and amplification of high power ultrashort pulses. The theoretical model given and tested for the SLA is clearly important for the understanding of these devices when used as amplifiers. Its utility, however, extends well beyond that. The results presented in Sect. 1 show that, when used in the hybrid mode-locked external cavity configuration, these devices can generate femtosecond pulses of record high power. It is also clear that these oscillators behave very differently from other mode-locked lasers. The details of the mode-locking mechanisms are currently not at all well understood. We have shown that very strong spectral changes occur in a single round trip inside the laser cavity. In particular, the spectrum of the internally circulating pulse is very different before and after passing through the SLA. This is because inside the laser cavity the SLA is operating in the high-gain, strong-saturation regime. Additionally, the unique feature of this laser is that it produces a relatively long pulse but with a nearly perfectly linear chirp resulting in $\approx$30 times excess coherent bandwidth, which allows external compression to femtosecond duration. Clearly, the equations that we have successfully tested for single-pass amplification can become the most important building blocks of a future theory for the mode-locked oscillator. In such a theory, the pulse evolution will be followed over many round trips, after suitable models for the external elements (saturable absorber, prism compensator etc.) are added. We intend to pursue the development of a theory of the mode-locked oscillator in the near future.

A final few remarks. The last few years have seen rapid advancement in ultrashort pulse technology. Solid-state lasers have all but replaced the venerable dye laser for femtosecond pulse generation. The development of the high average-power self-mode-locked Ti:Sapphire laser has overshadowed the equally impressive advances in mode locking of both integrated [6, 32] semiconductor lasers and of external cavity semiconductor lasers discussed in this paper. However, until an economical short-wavelength high-power diode-laser array becomes available, the Ti:Sapphire laser must be pumped by large, expensive, and inefficient ion lasers or other crystal-host lasers. The high pumping efficiency of diode lasers and their small size suggests that they may serve as possible alternatives in many applications. This paper has described the latest experimental and theoretical advances in high-power ultrashort-pulse semiconductor lasers and amplifiers. These lasers clearly have the potential for use not only in the research laboratory but also in high-speed optical signal processing and communication systems where small size, durability, and low operating cost are critical.

References

1. P.J. Delfyett, C.H. Lee, G.A. Alphonse, J.C. Connolly: Appl. Phys. Lett. **57**, 971 (1990)
2. P.J. Delfyett, L.T. Florez, N. Stoffel, T. Gmitter, N.C. Andreadakis, Y. Silberberg, J.P. Heritage, G.A. Alphonse: IEEE J. QE-**28**, 2203 (1992)
3. E.P.Ippen, D.J. Eilenberg, R.W. Dixon: Appl. Phys. Lett. **37**, 267 (1980)
4. J.P. van der Ziel, W.T. Tsang, R.A. Logan, R.M. Mikulyiak, W.M. Augustyniak: Appl. Phys. Lett. **39**, 525 (1981)
5. Y. Silberberg, P.W. Smith: IEEE J. QE-**22**, 759 (1986)
6. D.J. Derickson, R.J. Helkey, A. Mar, J.R. Karin, J.G. Wasserbauer, J.E. Bower: IEEE J. QE-**28**, 2186 (1992)
7. A.G. Weber, M. Schell, G. Fischbeck, D. Bimberg: IEEE J. QE-**28**, 2220 (1992)
8. M.S. Stix, M.P. Kesler, E.P. Ippen: Appl. Phys. Lett. **48**, 1722 (1986)
9. K.L. Hall, J. Mark, E.P. Ippen, G. Eisenstein: Appl. Phys. Lett. **56**, 1740 (1990)
10. C.T. Hultgren, E.P. Ippen: Appl. Phys. Lett. **59**, 635 (1991)
11. Y. Lai, K.L. Hall, E.P. Ippen: IEEE Photon. Tech. Lett. **2**, 711 (1990)
12. K.L. Hall, A.M. Darwish, E.P. Ippen, U. Koren, G. Raybon: Appl. Phys. Lett. **62**, 1320 (1993)
13. C.T. Hultgren, D.J. Dougherty, E.P. Ippen: Appl. Phys. Lett. **61**, 2767 (1992)
14. P.J. Delfyett, Y. Silberberg, G.A. Alphonse: Appl. Phys. Lett. **59**, 10 (1991)
15. J. Mark, J. Mørk: Appl. Phys. Lett. **61**, 2281 (1992)
16. G.A. Alphonse, D.B. Gilbert, M.G. Harvey, M. Ettenberg: IEEE J. QE-**24**, 2454 (1988)
17. E. Yablonovitch, T. Gmitter, J.P. Harbison, R. Bhat: Appl. Phys. Lett. **51**, 2222 (1987)
18. P.J. Delfyett, C.H. Lee, L.T. Florez, N.G. Stoffel, T.J. Gmitter, N.C. Andreadakis, G.A. Alphonse, J.C. Connolly: Opt. Lett. **15**, 1371 (1990)
19. G.P. Agrawal, N.A. Olsson: IEEE J. QE-**25**, 2297 (1989)
20. H.A. Haus, Y. Silberberg: J. Opt. Soc. Am. B **2**, 1237 (1985)
21. F. Krausz, M.E. Fermann, T. Brabec, P.F. Curley, M. Hofer, M.H. Ober, C. Spielmann, E. Wintner, A.J. Schmidt: IEEE J. QE-**28**, 2097 (1992)
22. A. Dienes, J.P. Heritage, M.Y. Hong, Y.H. Chang: Opt. Lett. **17**, 1602 (1992)

23. M.Y. Hong, Y.H. Chang, A. Dienes, J.P. Heritage, P.J. Delfyett: IEEE J. Quantum Electron. (in press)
24. K. Vahala, L.C. Chiu, S. Margalit, A. Yariv: Appl. Phys. Lett. **42**, 631 (1983)
25. A. Uskov, J. Mørk, J. Mark: IEEE Photon. Tech. Lett. **4**, 443 (1992)
26. M. Sheik-Bahae, D.J. Hagan, E.W. van Stryland: Phys. Rev. Lett. **65**, 96 (1990)
27. G.P. Agarwal, C.M. Bowden: IEEE Photon. Tech. Lett. **5**, 640 (1993)
28. E.W. van Stryland, M.A. Woodall, H. Vanherzeele, M.J. Soileau: Opt. Lett. **10**, 490 (1985)
29. M.J. LaGasse, K.K. Anderson, C.A. Wang, H.A. Haus, J.G. Fujimoto: Appl. Phys. Lett. **56**, 417 (1990)
30. C.B. Kim, E.T. Peng, C.B. Su, W. Rideout, G.H., Cha: IEEE Photon. Tech. Lett. **4**, 969 (1992)
31. J.P. Heritage, E.W. Chase, R.N. Thurnston, M. Stern: In *Proc. Conf. Lasers and Electro-Optics 1991* (Optical Society of America, Washington, DC 1991) p. 74
32. Y.K. Chen, M.C. Wu, T. Tanbun-Ek, R.A. Logan, M.A. Chin: Appl. Phys. Lett. **58**, 1253 (1991)